Efficient solid–shell finite elements for quasi-static and dynamic analyses and their application to sheet metal forming simulation

Peng WANG[1,a *], Hocine CHALAL[1,b] and Farid ABED-MERAIM[1,c]

[1] LEM3, UMR CNRS 7239 - Arts et Métiers ParisTech, 4, rue Augustin Fresnel, 57078 Metz Cedex 03, France

[a]Peng.WANG@ensam.eu, [b]Hocine.CHALAL@ensam.eu, [c]Farid.ABED-MERAIM@ensam.eu

Keywords: thin structures, linear and quadratic solid–shell finite elements, reduced integration, quasi-static, dynamic, sheet metal forming.

Abstract. Thin structures are commonly designed and employed in engineering industries to save material, reduce weight and improve the overall performance of products. The finite element (FE) simulation of such thin structural components has become a powerful and useful tool in this field. For the last few decades, much attention and effort have been paid to establish accurate and efficient FE. In this regard, the solid–shell concept proved to be very attractive due to its multiple advantages. Several treatments are additionally applied to the formulation of solid–shell elements to avoid all locking phenomena and to guarantee the accuracy and efficiency during the simulation of thin structures. The current contribution presents a family of prismatic and hexahedral assumed-strain based solid–shell elements, in which an arbitrary number of integration points are distributed along the thickness direction. Both linear and quadratic formulations of the solid–shell family elements are implemented into ABAQUS static/implicit and dynamic/explicit software to model thin 3D problems with only a single layer through the thickness. Two popular benchmark tests are first conducted, in both static and dynamic analyses, for validation purposes. Then, attention is focused on a complex sheet metal forming process involving large strain, plasticity and contact.

Introduction

The predictive simulation of thin sheet metal structures using the finite element method has played a significant role in product design and manufacture processes. In order to obtain reliable simulation results, considerable effort has been devoted to the development of solid–shell FE during the last few decades [1-4]. These elements combine the advantages of the more traditional solid and shell elements. They are based on a classical three-dimensional formulation with reduced integration and enhanced strain fields. In the present work, a family of solid–shell (SHB) elements is presented. It consists of linear hexahedral (SHB8PS) and prismatic (SHB6) elements and their quadratic versions (SHB20 and SHB15, respectively) [5-8]. All of these FE are implemented into ABAQUS in both versions: static/implicit and dynamic/explicit software packages, which provide a library of efficient elements capable of solving most of thin structure problems. In this paper, the basic formulation of the SHB elements is summarized first; then, two popular benchmark tests and one related to sheet metal forming processes are chosen to assess the performance of these SHB elements.

Formulation of the SHB solid–shell elements

In this section, the basic formulation of all SHB solid–shell elements is briefly introduced. The detailed formulation of the SHB elements can be found in [3,5-8].

Geometry and integration points. The geometry and location of integration points for SHB8PS, SHB6, SHB20, and SHB15 elements are shown in Fig. 1. The special direction ζ is chosen to represent the thickness direction, along which an arbitrary number of integration points can be arranged. Usually, for non-linear tests involving large strain and plasticity, which is the case of the benchmark tests in this paper, five integration points through the thickness are recommended [5].

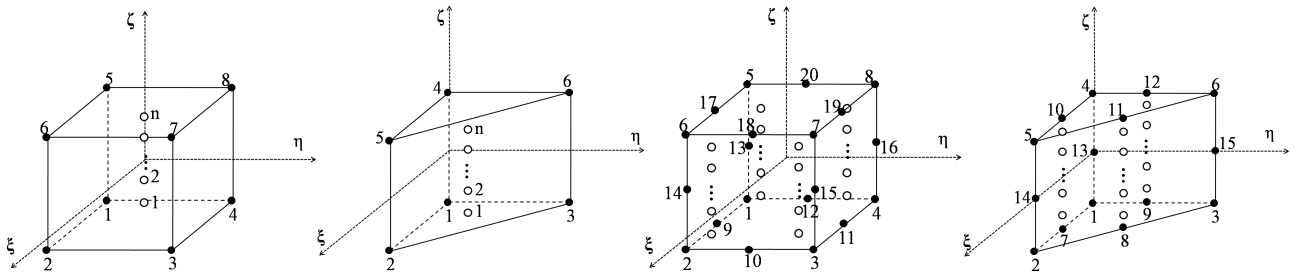

(a) SHB8PS (b) SHB6 (c) SHB20 (d) SHB15

Fig. 1. Geometry of the SHB elements and location of integration points: (a) linear 8-node hexahedral element, (b) linear 6-node prismatic element, (c) quadratic 20-node hexahedral element and (d) quadratic 15-node prismatic element.

General formulation of quasi-static versions. The SHB solid–shell elements are based on a 3D approach using the classical isoparametric linear and quadratic shape functions for standard hexahedral and prismatic elements. The coordinates x_i and displacements u_i inside an element are interpolated using the shape functions N_I and the nodal displacements d_{iI} as follows:

$$x_i = x_{iI} N_I(\xi,\eta,\zeta) = \sum_{I=1}^{n} N_I(\xi,\eta,\zeta) x_{iI}\,, \tag{1}$$

$$u_i = d_{iI} N_I(\xi,\eta,\zeta)\,, \tag{2}$$

where the lowercase subscript *i* varies from 1 to 3 and represents the spatial coordinate directions; the uppercase subscript *I* goes from 1 to *n*, where *n* denotes the number of element nodes.

Based on the interpolation of the displacement field (Eq. 2), the strain field $\nabla_s(u)$ is related to the nodal displacement field $\mathbf{d} = \left(\mathbf{d}_1, \mathbf{d}_2, \mathbf{d}_3\right)^T$, with $\mathbf{d}_i = \left(d_{i1}, ..., d_{in}\right)$, by the following relationship:

$$\nabla_s(u) = \mathbf{B} \cdot \mathbf{d}\,, \tag{3}$$

where $\mathbf{B}$ is the discrete gradient operator, whose matrix representation has a size of 6×3*n*.

The assumed-strain method used in the formulation of the SHB elements is based on the simplified form of the Hu–Washizu principle, as introduced by Simo and Hughes [9]

$$\pi(\dot{\bar{\boldsymbol{\varepsilon}}}) = \int_{\Omega_e} \delta\dot{\bar{\boldsymbol{\varepsilon}}}^T \cdot \boldsymbol{\sigma}\; d\Omega - \delta\dot{\mathbf{d}}^T \cdot \mathbf{f}^{ext} = 0\,, \tag{4}$$

where δ denotes a variation, $\dot{\bar{\boldsymbol{\varepsilon}}}$ the assumed-strain rate, $\boldsymbol{\sigma}$ the stress field, $\dot{\mathbf{d}}$ the nodal velocities, and $\mathbf{f}^{ext}$ the external nodal forces. The assumed-strain rate $\dot{\bar{\boldsymbol{\varepsilon}}}$, represented by a six-component vector, is expressed in terms of a $\overline{\mathbf{B}}$ matrix, projected from the classical discrete gradient $\mathbf{B}$ defined by Eq. 3

$$\dot{\bar{\boldsymbol{\varepsilon}}}(x,t) = \overline{\mathbf{B}}(x) \cdot \dot{\mathbf{d}}(t)\,. \tag{5}$$

Substituting the above equation into the variational principle (Eq. 4), the stiffness matrix $\mathbf{K}_e$ and the internal force $\mathbf{f}^{\text{int}}$ can be defined as

$$\mathbf{K}_e = \int_{\Omega_e} \overline{\mathbf{B}}^T \cdot \mathbf{C}^{ep} \cdot \overline{\mathbf{B}}\; d\Omega + \mathbf{K}_{GEOM}\,, \qquad \mathbf{f}^{\text{int}} = \int_{\Omega_e} \overline{\mathbf{B}}^T \cdot \boldsymbol{\sigma}\; d\Omega\,, \tag{6}$$

where the geometric stiffness matrix $\mathbf{K}_{GEOM}$ is due to the non-linear (quadratic) part of the strain tensor (see [5] for more details). $\mathbf{C}^{ep}$ represents the elastic–plastic tangent modulus of the constitutive law.

The equations outlined above summarize the basic structure of the SHB solid–shell elements. It is worth noting that an extra special stabilization treatment, which is calculated in the co-rotational coordinate frame [5], is needed in the formulation of SHB8PS to control the hourglass modes. For the SHB6 element, it has been shown that its formulation does not induce hourglass modes, but an appropriate projection of the strains is required to eliminate some locking phenomena [6]. For the SHB20 and SHB15 elements, no additional special treatment in the formulation is needed [8].

Formulation of dynamic versions. The main algorithm and the general structure for the dynamic versions of the SHB elements are similar to those developed in the quasi-static versions, which are not repeated here. In the dynamic versions, new variables such as the velocity field $\boldsymbol{\upsilon}$ and strain rate field $\dot{\boldsymbol{\varepsilon}}$ need to be defined in the same way as the displacement and strain fields defined above. Moreover, only the mass matrix is involved in explicit dynamic simulations, while the stiffness matrix is not required in the element formulations. Several methods are available in the literature to compute the mass matrix (see, e.g., [10]). Here, the diagonal lumped element mass matrix $\mathbf{M}^e$ is adopted for all SHB elements, which derives from the following bloc of components:

$$\mathrm{M}_{IJ} = \begin{cases} m\int_\Omega \rho N_I N_J d\Omega & I = J \\ 0 & I \neq J \end{cases}, \qquad \text{with} \quad m = \int_\Omega \rho d\Omega \Big/ \sum_{I=1}^{n} \int_\Omega \rho N_I N_I d\Omega \tag{7}$$

where N_I and N_J are the shape functions and ρ is the material density. The lumped mass matrix $\mathbf{M}^e$, with a size of $3n\times3n$, is obtained by repeating Eq. 7 in three equal parts.

Numerical examples and results

Non-linear quasi-static test. A free cylinder pulled by a pair of radial forces is considered, which involves both geometric and material non-linearities. All geometric dimensions and elasto-plastic material parameters are taken from [11,12], as summarized in Fig. 2(a). Due to the symmetry, only one eighth of the cylinder is modeled. This test is simulated using the arc-length procedure. The load–displacement curves given by the SHB elements at points A and B are reported in Fig. 2(b) and compared to those obtained in [11,12]. The results of the SHB elements are in good agreement with the reference results, except for the linear prismatic SHB6 element where a finer mesh is required to obtain a more accurate solution for the displacement of point B.

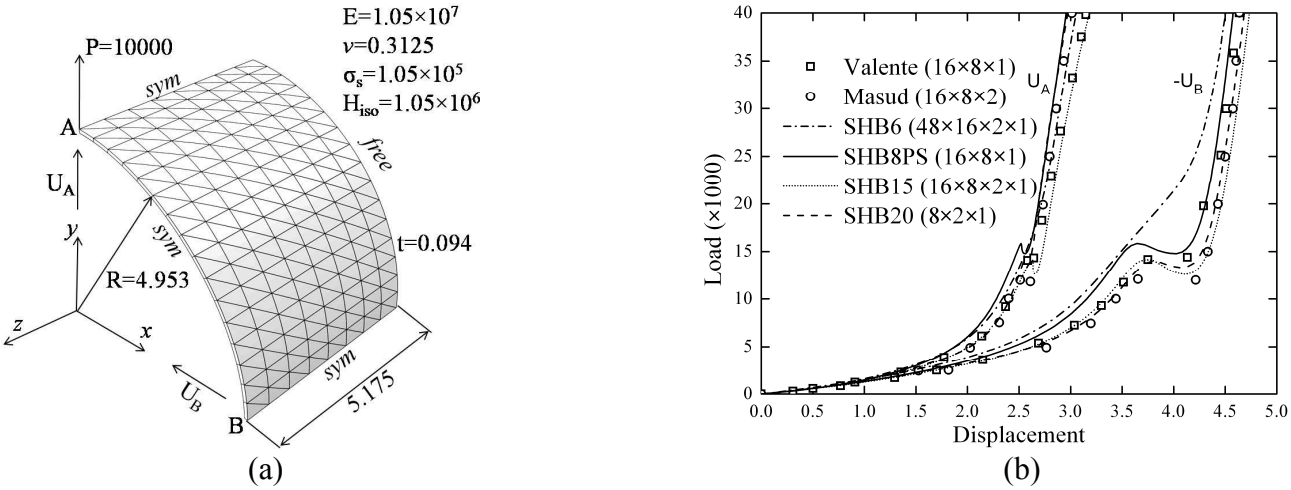

Fig. 2. Geometry (a) and load–displacement curves (b) for the stretched cylinder.

Non-linear dynamic test. A fully clamped perfectly elasto-plastic plate is impulsively loaded over the whole plate surface with an initial velocity of 35,000 mm/s. This test has been considered in [13] in the case of dynamic-explicit analysis. All geometric and material parameters are provided in Fig. 3(a). According to the symmetry of the problem, only one quarter of the plate is modeled.

The vertical displacement history curves at the center point A (see Fig. 3(a)) obtained by the SHB elements are shown in Fig. 3(b) and compared to the results presented in [13]. This figure shows a better agreement with the results given in [13] when the quadratic SHB elements are used for this special case of dynamic problem involving high velocity-type loading.

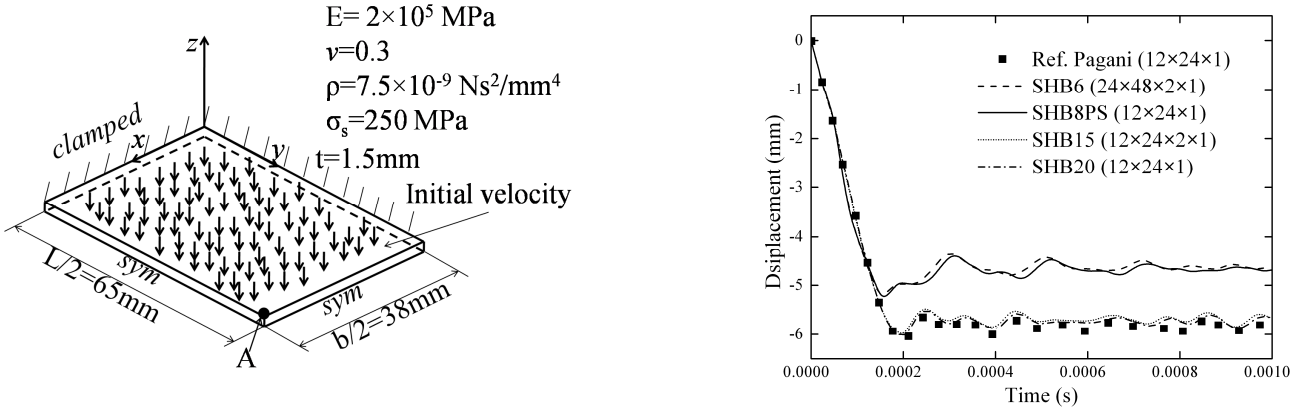

(a) (b)

Fig. 3. Geometry (a) and displacement history (b) for the explosively loaded rectangular plate.

Simulation of sheet metal forming process. The deep drawing of a square cup proposed in [14] is considered here to evaluate the performance of the SHB elements. The geometric dimensions of the forming tools are illustrated in the schematic view of Fig. 4.

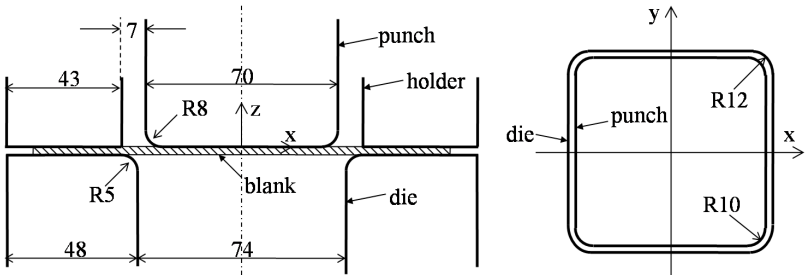

Fig. 4. Schematic view of the square cup drawing process.

An initial aluminum square sheet of 150×150×0.81 mm is considered for the simulations. The associated elastic–plastic material parameters are reported in Table 1, where the Swift law is considered to describe the isotropic hardening

$$\sigma_y = k(\varepsilon_0 + \varepsilon_{eq}^p)^n \tag{8}$$

A constant blank holder force of 16.6 kN is applied during the forming process [14]. The friction coefficient between the blank and the forming tools is taken equal to 0.162 [14]. Only one quarter of the square cup model is analyzed due to the symmetry of the problem. The deformed blank, corresponding to the final punch stroke of 15 mm, is illustrated in Fig. 5 for all SHB elements.

Table 1. Elastic–plastic parameters for the studied aluminum alloy.

	E [MPa]	ν	k [MPa]	ε_0	n
Aluminum	71,000	0.33	576.79	0.01658	0.3593

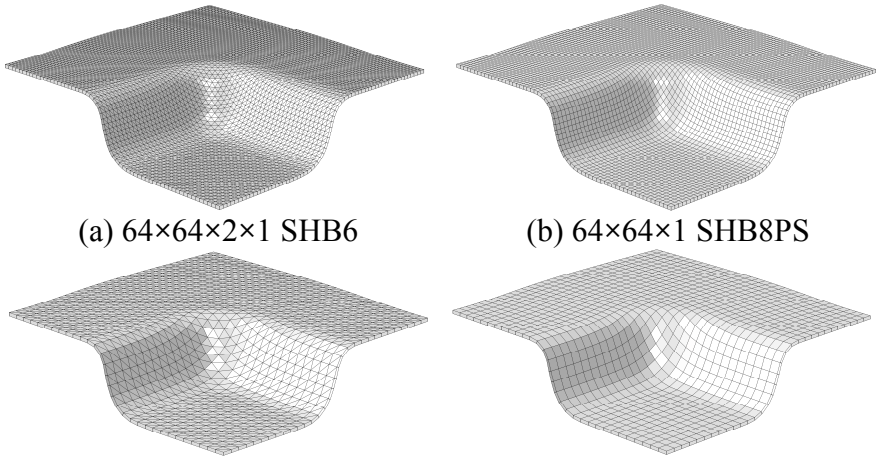

(a) 64×64×2×1 SHB6 (b) 64×64×1 SHB8PS

(c) 32×32×2×1 SHB15 (d) 32×32×1 SHB20

Fig. 5. Final deformed shape of the blank at 15 mm punch stroke using the SHB elements.

Both static/implicit and dynamic/explicit versions of the SHB elements are used for the simulations and all results are compared to the experimental ones provided in [14]. The final draw-in measurements of the formed blank at 15 mm punch stroke are listed in Table 2, where D_x denotes the draw-in distance along the x-axis, D_y along the y-axis and D_d the draw-in distance along the diagonal direction. It can be noted that the D_x and D_y draw-in distances predicted by the implicit version of SHB elements are identical, which is consistent with the isotropic plastic behavior of the sheet, while the explicit version of SHB elements predicts slightly different draw-in distances between the x and y directions. In the latter, very small time increments are required to obtain accurate results as compared to implicit analysis, where the global equilibrium is enforced after each loading increment thus allowing relatively large time increments. On the whole, a good agreement is obtained between the implicit and explicit results of the SHB elements, and almost all of the simulated results lie in the interval defined by the minimum and maximum draw-in experimental measurements.

Table 2. Draw-in distances at 15 mm punch stroke: comparison between simulations and experiments.

	Mesh	Version	D_x [mm]	D_y [mm]	D_d [mm]
Min. experiment	———	———	3.80	3.90	2.30
Max. experiment	———	———	6.45	6.49	3.79
SHB6	64×64×2×1	implicit	5.44	5.44	2.63
SHB6	64×64×2×1	explicit	5.78	5.92	3.11
SHB8PS	64×64×1	implicit	5.89	5.89	3.15
SHB8PS	64×64×1	explicit	6.16	6.07	3.20
SHB15	32×32×2×1	implicit	5.91	5.91	3.08
SHB15	32×32×2×1	explicit	6.45	6.45	3.43
SHB20	32×32×1	implicit	5.61	5.61	2.32
SHB20	32×32×1	explicit	7.11	7.23	1.95

Summary

In this work, linear hexahedral and prismatic solid–shell (SHB) elements, as well as their quadratic counterparts, have been proposed to model thin 3D structures. Several numerical treatments, such as the reduced integration technique, stabilization and specific projections of the strains, are adopted in the formulation to eliminate the locking phenomena that usually appear in thin-structure simulations. Thanks to these treatments, the SHB elements are expected to be capable of solving complex problems, involving geometric, material and contact non-linearities, in both quasi-static and dynamic analyses. All linear and quadratic SHB elements have been successfully implemented into the implicit

and explicit ABAQUS codes. The performance of the proposed SHB elements was first demonstrated through two non-linear elastic–plastic static and dynamic tests, involving large displacements and rotations. Then, the deep drawing of a square cup of aluminum alloy sheet was conducted via both static and dynamic analyses to further evaluate their ability to model sheet metal forming processes using a single layer of FE through the thickness. On the whole, comparisons between the simulation results and the experiments revealed good agreement. As shown by the numerical tests, the implicit versions of the SHB elements are accurate and suitable for application to most quasi-static problems, while the explicit versions enable modeling of impact problems as well as complex sheet metal forming processes involving severe non-linearities that are difficult to handle with implicit analysis.

References

[1] R. Hauptmann, K. Schweizerhof, A systematic development of solid-shell element formulations for linear and nonlinear analyses employing only displacement degrees of freedom, Int. J. Num. Meth. Engng. 42 (1998) 49-70.

[2] K. Sze, L. Yao, A hybrid stress ANS solid-shell element and its generalization for smart structure modeling. Part I: solid-shell element formulation, Int. J. Num. Meth. Engng. 48 (2000) 545-564.

[3] F. Abed-Meraim, A. Combescure, SHB8PS - a new adaptive, assumed-strain continuum mechanics shell element for impact analysis, Computers and Structures. 80 (2002) 791-803.

[4] G. Cocchetti, M. Pagani, U. Perego, Selective mass scaling and critical time-step estimate for explicit dynamics analyses with solid-shell elements, Computers and Structures. 127 (2013) 39-52.

[5] F. Abed-Meraim, A. Combescure, An improved assumed strain solid–shell element formulation with physical stabilization for geometric non-linear applications and elastic–plastic stability analysis, Int. J. Num. Meth. Engng. 80 (2009) 1640-1686.

[6] V. Trinh, F. Abed-Meraim, A. Combescure, A new assumed strain solid–shell formulation "SHB6" for the six-node prismatic finite element, J. Mech. Sci. Tech. 25 (2011) 2345-2364.

[7] A. Salahouelhadj, F. Abed-Meraim, H. Chalal, T. Balan, Application of the continuum shell finite element SHB8PS to sheet forming simulation using an extended large strain anisotropic elastic–plastic formulation, Arch. App. Mech. 82 (2012) 1269-1290.

[8] F. Abed-Meraim, V. Trinh, A. Combescure, New quadratic solid–shell elements and their evaluation on linear benchmark problems, Computing. 95 (2013) 373-394.

[9] J.C. Simo, T.J.R. Hughes, On the variation foundations of assumed strain methods, J. Appl. Mech. 53 (1986) 51-54.

[10] O.C. Zienkiewicz, R.L. Taylor, J.Z. Zhu, The Finite Element Method, sixth ed., Elsevier Ltd. 2006.

[11] A. Masud, C.L. Tham, Three-dimensional corotational framework for finite deformation elasto-plastic analysis of multilayered composite shells. AIAA Journal. 38 (2000) 2320-2327.

[12] R.A. Fontes Valente, R.J. Alves de Sousa, R.M. Natal Jorge, An enhanced strain 3D element for large deformation elastoplastic thin-shell applications, Computational Mechanics. 34 (2004) 38-52.

[13] M. Pagani, S. Reese, U. Perego, Computationally efficient explicit nonlinear analyses using reduced integration-based solid-shell finite elements, Comput. Meth. Appl. Mech. Engng. 268 (2014) 141-159.

[14] A. Makinouchi, E. Nakamachi, E. Oñate, R.H. Wagoner, NUMISHEET'93, Proceedings of the 2nd International Conference and Workshop on Numerical Simulation of 3D Sheet Metal Forming Processes - Verification of Simulation with Experiment, Isehara, Japan, 1993.